Manipulating the extraordinary acoustic transmission through metamaterial-based acoustic band gap structures

Cite as: Appl. Phys. Lett. **104**, 161906 (2014); https://doi.org/10.1063/1.4873391
Submitted: 17 February 2014 . Accepted: 15 April 2014 . Published Online: 23 April 2014

N. Aközbek, N. Mattiucci, M. J. Bloemer, M. Sanghadasa, and G. D'Aguanno

Manipulating the extraordinary acoustic transmission through metamaterial-based acoustic band gap structures

N. Aközbek,[1] N. Mattiucci,[1] M. J. Bloemer,[2] M. Sanghadasa,[2] and G. D'Aguanno[1,a)]
[1]*AEgis Tech., Nanogenesis Division 410 Jan Davis Dr, Huntsville, Alabama 35806, USA*
[2]*Department of the Army, Charles M. Bowden Facility, Redstone Arsenal, Alabama 35898, USA*

(Received 17 February 2014; accepted 15 April 2014; published online 23 April 2014)

We report theoretical predictions and experimental results on the formation of pass bands and stop bands of extraordinary acoustic transmission in multilayer structures based on alternating layers of acoustic metamaterial and air. The metamaterial layers can be made of any acoustically hard material perforated with a two-dimensional array of subwavelength apertures. In this way, it is possible to tailor the density and speed of sound of an otherwise acoustically bulk hard material with fixed properties. The sonic band structure allows transmission passband and stop bandgaps that depend on the layer thicknesses and effective properties of the metamaterials. In addition, we show the existence of resonant tunneling due to the formation of an acoustic passband in a spectral region of low transmission for a single layer. This opens the possibility to engineer different types of phononic materials to manipulate and control acoustic waves. © *2014 AIP Publishing LLC*. [http://dx.doi.org/10.1063/1.4873391]

Acoustic band gap materials are artificial materials that exhibit forbidden band gaps to sound waves in analogy to photonic band gaps for light waves. For light waves, the band structure originates from the periodic variation of the refractive index,[1] and likewise for sound waves, a periodic variation of the material's density can give rise to acoustic pass bands and stop bands. Acoustic band gap materials have been widely studied in the past[2–4] due to the plethora of possible applications in acoustic insulation, acoustic filtering, and nonlinear acoustics. Unlike in optics, where many solid optically transparent materials exist, for acoustic waves most solid bulk materials are not transparent to sound waves. In this regard, most studies on acoustic band gap materials have been limited to 2D structures made of cylinder scatters.[2] Recently, a new class of artificial materials, so called metamaterials (MMs), has emerged in which the material properties are manipulated by embedded resonant inclusions such as Helmholtz resonators or core shell particles, in an acoustically soft host medium whose periodicity and size is much less than the wavelength. In this case, the composite material can be described by effective bulk properties. One limitation of this approach is the losses associated with the intrinsic nature of the resonance condition. Another approach is using subwavelength apertures in an acoustically hard material. This allows tailoring an acoustic metamaterial with desired densities and speed of sound of an otherwise acoustically hard material by simply changing the percentage of the open area of the hole array. In a recent publication,[5] it has been demonstrated that a slab of acoustically hard material (i.e., impenetrable to sound waves) periodically perforated with a two-dimensional array of subwavelength apertures of period d_x and d_y, area of the elementary cell $S_1 = d_x \times d_y$ and area of the apertures S_2 (see Fig. 1), can be homogenized as a MM slab with effective, spatially dispersive, constitutive parameters given by the following equations:

$$c_{MM} = c_{air}/\sqrt{1+\sin^2\vartheta},\ \rho_{MM} = \rho_{air}S_1/S_2, \qquad (1)$$

where c_{air} and ρ_{air} are, respectively, the sound velocity in air (343 m/s) and the density of air (1.21 kg/m^3), ϑ is the incident angle of the sound wave with respect to the normal to the slab's surface. Equation (1) does not contain the density of the plate since we are considering only acoustically hard materials. The homogenization procedures for such kind of perforated slab have also been analyzed, subsequently to Ref. 5, in Refs. 6 and 7. The acoustically hard material effectively becomes a "soft" material with sound velocity comparable with the speed of sound in air and density equal to the density of air enhanced by a factor that is the inverse of the open area (S_2/S_1). For example, an aluminum plate ($\rho_{Al} = 2700$ kg/m^3, $c_{Al} = 6300$ m/s) with only 20% open area would have at normal incidence effective acoustic parameters: $\rho_{MM} = 5\rho_{Air} = 6$ kg/m^3, $c_{MM} = c_{air} = 343$ m/s, i.e., a reduction of almost four orders of magnitude in the effective acoustic impedance ($Z_{ac} = \rho c$) with respect to the solid plate with no perforation. Equation (1) is valid under the assumption that the grating periodicity is smaller than the sound wavelength ($\lambda > 2d_x$, $\lambda > 2d_y$) so that all diffraction orders, except the zeroth, are evanescent. Moreover, in Ref. 5, it has also been demonstrated that the slab admits an intromission angle ϑ_I at $\cos\vartheta_I = S_2/S_1$, similar to the Brewster angle in optics, where broadband impedance matching and complete transmission of acoustic waves is achieved.

In this Letter, we study the band gap structure and the transmission properties of one-dimensional acoustic multilayers based on alternating layers of acoustic MM and air, as schematically sketched in Fig. 1. A key distinction of this approach is that it allows the observation of pass bands and stop bands over audible frequencies in air using acoustically hard materials which is otherwise not possible to achieve due to large impedance mismatch. We also show enhanced transmission bands when compared to the transmission with a single plate. Following the same approach used for

a)Author to whom correspondence should be addressed. Electronic addresses: giuseppe.daguanno@us.army.mil and gdaguanno@nanogenesisgroup.com.

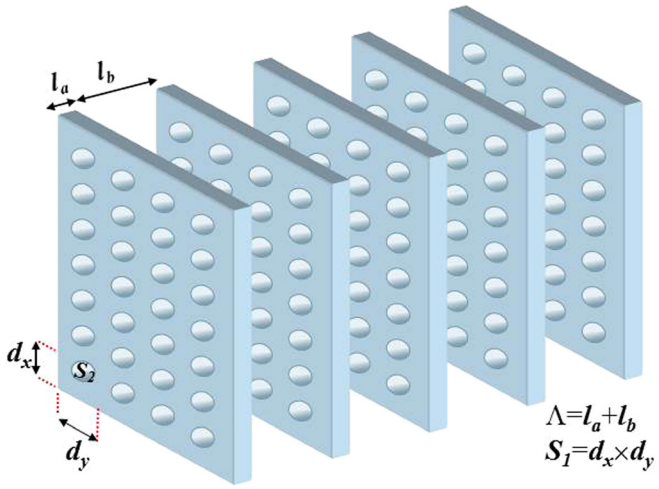

FIG. 1. Acoustic multilayer structure made of alternating layers of air and an acoustically hard material perforated with a two-dimensional array of subwavelength holes.

infinitely periodic photonic structures,[1] the dispersion relation of an acoustic wave propagating in an acoustic band gap structure can be calculated through the Bloch vector of the structure by applying Floquet's theorem. The spectral regions in which the Bloch vector is purely real determine the allowed bands, while the spectral regions in which the Bloch vector has an imaginary part correspond to the forbidden bands where only evanescent modes are allowed. In particular, for a one-dimensional periodic multilayer of infinite length the acoustic Bloch vector can be simply calculated, in analogy with the electromagnetic case,[8] by the trace of the transfer matrix $\hat{M}$ of the elementary cell as:[4] $\cos(K_\beta\Lambda) = (1/2)Tr(\hat{M})$ which, in the case of an elementary cell made of two acoustic materials (a,b) with density and sound velocity, respectively, (ρ_a,c_a) and (ρ_b,c_b), takes the following simple expression:

$$\cos(K_\beta\Lambda) = \cos(q_a l_a)\cos(q_b l_b) - \frac{1}{2}\left(\frac{q_a\rho_b}{q_b\rho_a}+\frac{q_b\rho_a}{q_a\rho_b}\right)\sin(q_a l_a)\sin(q_b l_b), \quad (2)$$

where $q_{a,b} = \sqrt{(\omega/c_{a,b})^2 - k_\parallel^2}$ and $k_\parallel = (\omega/c_{air})\sin\vartheta$ is the component of the incident wavevector parallel to the interface, and $\omega = 2\pi\nu$ is the angular frequency of the incident wave. In our case, the layer a is the acoustic MM characterized by the effective parameters (1) and the layer b is air, so that the expression of the Bloch vector becomes

$$\cos(K_\beta\Lambda) = \cos\left(\frac{\omega l_a}{c_{air}}\right)\cos\left(\frac{\omega l_b\cos\vartheta}{c_{air}}\right) - \frac{1}{2}\left(\frac{S_2}{S_1\cos\vartheta}+\frac{S_1\cos\vartheta}{S_2}\right)\sin\left(\frac{\omega l_a}{c_{air}}\right)\sin\left(\frac{\omega l_b\cos\vartheta}{c_{air}}\right). \quad (3)$$

Equation (3) tells us that in this case the band structure depends only on the geometrical characteristics of the sample, i.e., the percentage of the open area of the metamaterial layer S_2/S_1, the layer thicknesses l_a and l_b, and the angle of incidence ϑ. Moreover, the sample admits the same intromission angle condition as the single MM layer, in fact for $\cos\vartheta_I = S_2/S_1$ the expression (3) of the Bloch vector becomes linearly dependent on the frequency

$$K_\beta = \frac{(l_a + l_b S_2/S_1)}{\Lambda}\frac{\omega}{c_{air}}, \quad (4)$$

as if the sound wave were propagating in a homogeneous, non-dispersive, non-absorbing acoustic material with effective velocity $c_{eff} = c_{air}\Lambda/(l_a + l_b S_2/S_1)$. In Fig. 2, we show an example of the acoustic band gap structure calculated at normal incidence for different values of MM layer open area (S_2/S_1).

It is evident from Figure 2 that a wide range of possibilities exists to manipulate at will the position and the width of the band gaps by simply changing the open area of the metamaterial layers and/or the ratio l_b/l_a. As an example, in Fig. 2(c), we report the case in which the air layer is ten times longer than the metamaterial layer (dashed line) and the case in which they have equal thickness (dotted line). In the first case, the low frequency band gap is narrower than the high frequency band gap, while in the latter case the two band gaps have identical width and are symmetrically placed with respect to the frequency range reported. Fig. 3 shows the actual transmittance vs. frequency for the two cases considered for a finite, N = 6 period structure, the figure also shows the imaginary part of the Bloch vector which perfectly coincides with the position of the band gaps that were numerically calculated for the finite structure. The transmittance has been calculated using a standard transfer matrix technique in which the perforated layers are modeled through the effective parameters given by Eq. (1). In agreement with the previous study, it is noticed the symmetric

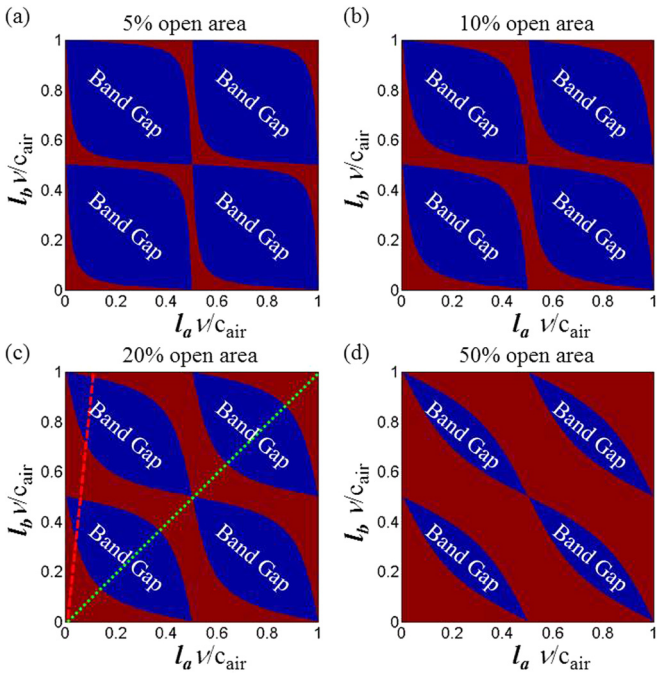

FIG. 2. Acoustic band gap for an infinite lattice calculated at normal incidence for different values of the open area of the MM layers. In Fig. 2(c), the straight lines correspond, respectively, to $l_a = 0.1\ l_b$ (dashed line) and $l_a = l_b$ (dotted line). The red regions correspond to the pass bands where the Bloch vector is purely real, while the blue regions correspond to the band gaps where its imaginary part is nonzero.

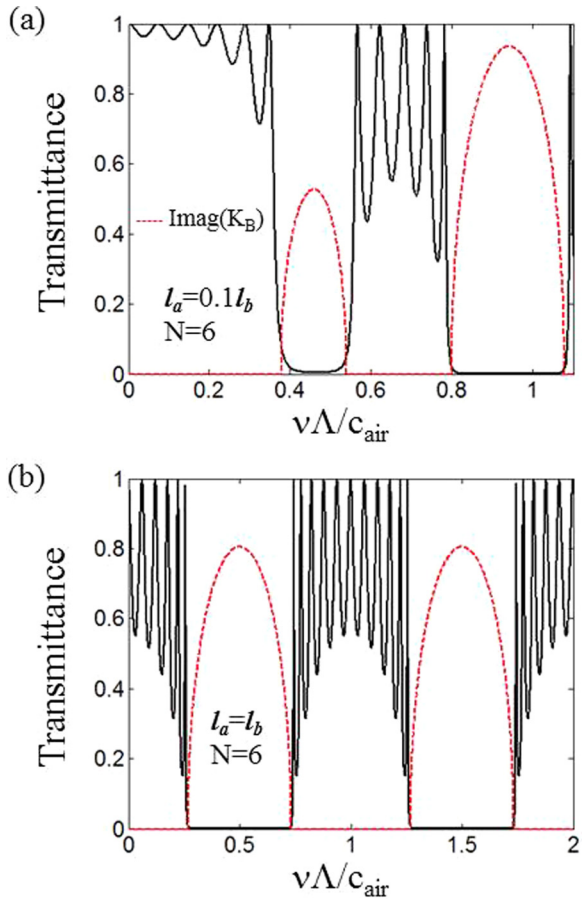

FIG. 3. (a) Transmittance (continuous line) vs. frequency for an N = 6 period structure with $S_2/S_1 = 20\%$ and $l_a = 0.1\ l_b$. Also plotted is the imaginary part of the Bloch vector (dashed line) for an infinite lattice, (b) same as in (a) for $l_a = l_b$.

position of the two identical band gaps for the case $l_a = l_b$ in contrast with the asymmetric position and different widths of the two band gaps in the case $l_a = 0.1\ l_b$.

In Fig. 4, we show the Bloch vector (upper panel) and the transmittance (lower panel) in the (ν,ϑ) plane for the same structures as in Fig. 3.

In the lower panel, the horizontal dashed line indicates the position of the intromission angle located at $\vartheta_I = \text{acos}(S_2/S_1) \cong 78^\circ$ where perfect, broadband transmission is achieved in analogy with the results reported in Ref. 5 for the single layer. It is worthwhile to note how the angular dispersion of the band gaps is much stronger for the case $l_a = 0.1\ l_b$, the right column of Fig. 4, i.e., when the air layers are much longer that the MM layers. This is due to the fact that the accumulated phase is dependent on the incident angle only for the air layers, as it is seen from Eq. (3). It is also interesting to underline how the angular acceptance of the intromission angle band can be narrowed (lower panel, left figure) or widened (lower panel, right figure) by varying the ratio l_b/l_a adding therefore an extra degree of control to the results reported in Ref. 5.

In order to verify experimentally the above theoretical predictions, we have performed transmission measurements in the range 2 kHz–20 kHz at normal incidence on several samples placed in an acoustic anechoic chamber. A sketch of the acoustic chamber, a picture of its interior and a picture of one of the samples is shown in Fig. 5.

For transmission measurements the chamber is divided into two parts, one where the speaker is located for sound generation and the other one where the transmitted sound through the test sample is detected via a microphone. We used a planar driver that operates from 500 Hz to 20 kHz. The microphone is a Bruel & Kjaer multi-field 1/4 in. microphone (type 4961) with frequency response from 20 Hz to 20 kHz. We used a BMS 4512ND 4 in. Neodymium planar wave driver. The driver is connected to a Crown XTi1000 amplifier. Data acquisition and analysis are done using the Bruel & Kjaer Pulse lab shop software. The transmittance experimentally measured is defined as $T_{sample}/T_{reference}$,

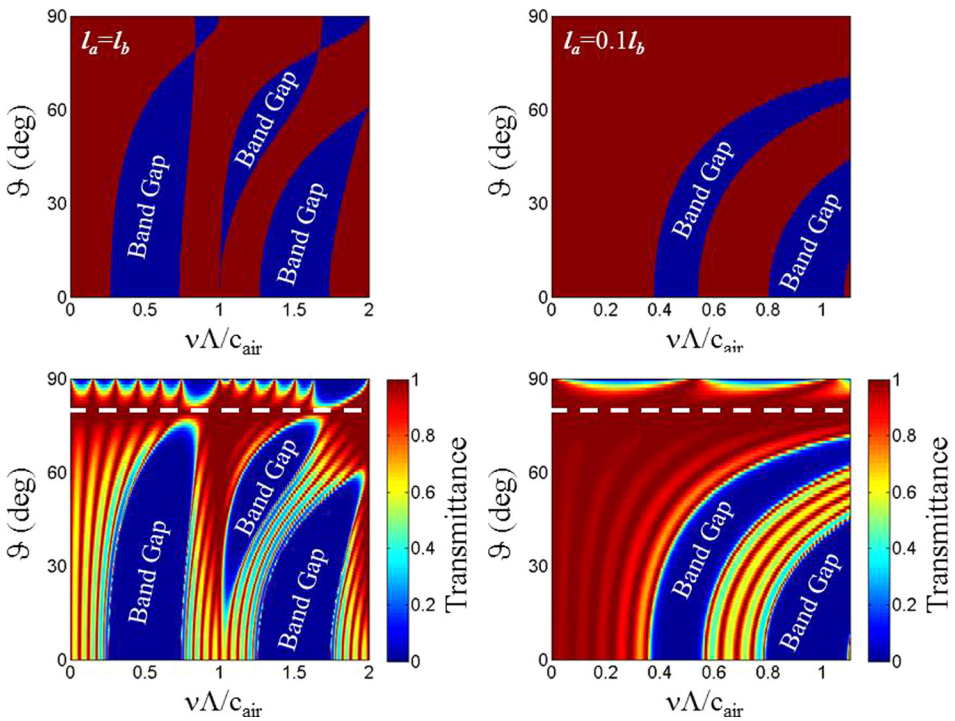

FIG. 4. Bloch vector for an infinite lattice (upper panel), analogous to Fig. 2, and transmittance of a 6 period structure (lower panel) in the (ν,ϑ) plane. The structures are the same as in Fig. 3, open area $S_2/S_1 = 20\%$, left column $l_a = l_b$, and right column $l_a = 0.1\ l_b$. In the lower panel, the horizontal dashed line represents the intromission angle located at $\vartheta_I = \text{acos}(S_2/S_1) \cong 78^\circ$ and the corresponding intromission band.

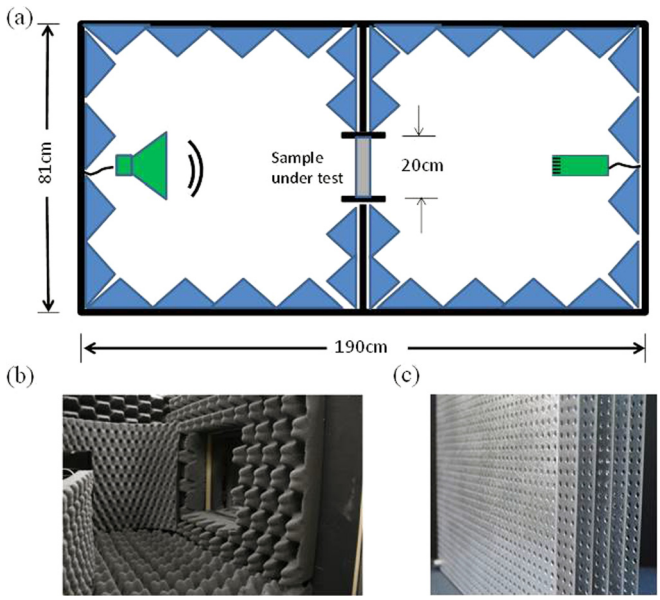

FIG. 5. (a) Sketch of the anechoic chamber. The two sections of the chamber are isolated so that sound is only transmitted through the sample under test through a 20 × 20 cm aperture. (b) Picture of the interior of the acoustic chamber. (c) Picture of one of the samples. The samples are made of aluminum plates ($l_a = 1.2$ mm) separated by air gaps ($l_b = 12.8$ mm). The aluminum plates are perforated with a periodic array of holes ($d_x = d_y = 7.9$ mm) with diameter 3.9 mm for a total open area $S_2/S_1 \cong 19\%$. The samples tested range from N = 1 to N = 6 periods.

where $T_{reference}$ is the transmittance without the sample in place. The experimental results for N = 1, 2, 3, 4, 5, and 6 period samples and the comparison with the theory are shown in Fig. 6.

The theory and the experiment show good agreement, in particular, we note that both the formation of the band gaps in the 8 kHz–12 kHz and above 18 kHz and the Fabry-Perot-like transmission resonances in the pass bands are well recaptured by the theory. As already mentioned, the theoretical calculations have been done using a matrix transfer technique in which the perforated layers are modeled through the MM effective parameters of Eq. (1). Here, however, we have considered in the calculation thicker aluminum layers than their actual dimension (2 mm instead of 1.2 mm) in order to compensate for a small shift between the calculated and measured position of the band gap and pass bands. This small shift is a known effect[5] associated with the evanescent higher diffraction orders excited at the grating interfaces and not taken into account in the effective parameter description of Eq. (1). Even for thicker plates, as in the case of Ref. 5, the correction in the thickness remains of the order of a fraction of millimeter. Moreover, in order to model the unavoidable losses due to sound absorption near each metal/air interface, we have also introduced at each metal/air interface a thin absorbing layer of air (0.2 mm thick) characterized by a complex sound velocity $c = c_{air}(1 - i\delta/\nu)$ as in Ref. 9 with the loss term here taken at $\delta = 10^3$ Hz.

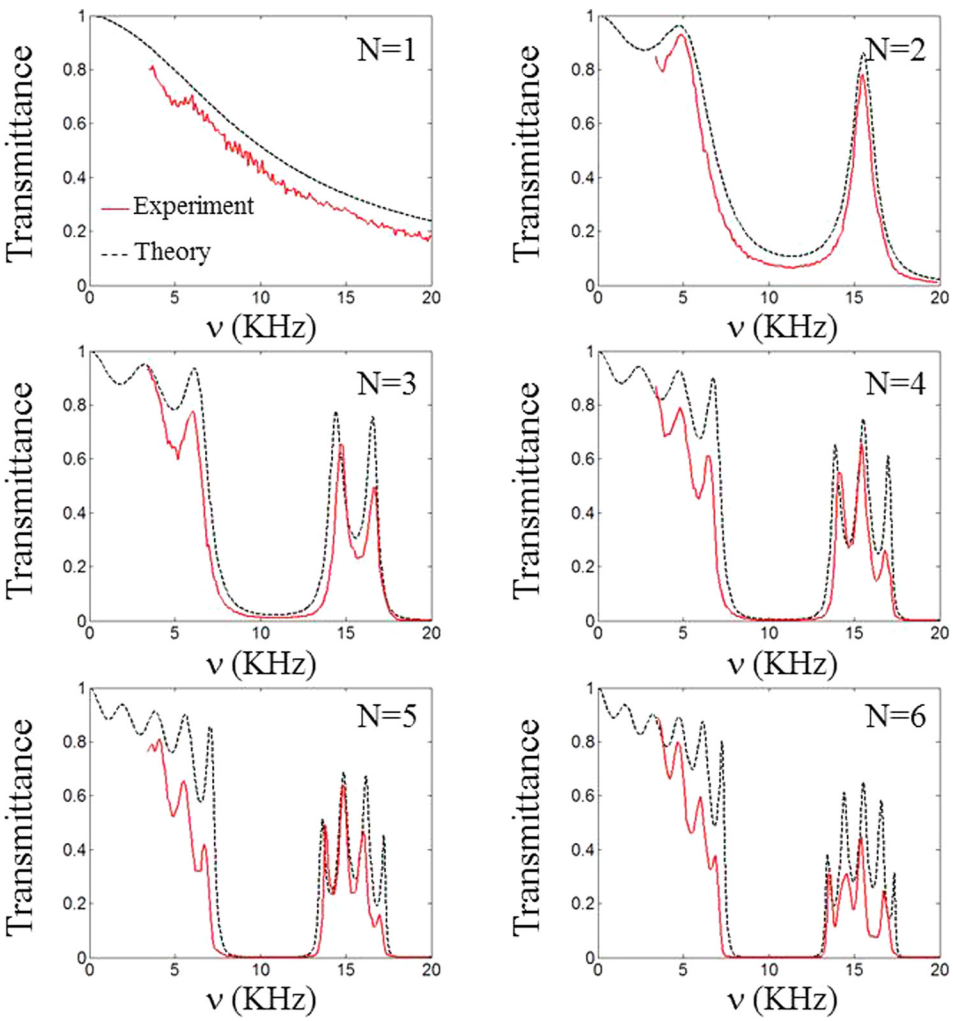

FIG. 6. Transmittance vs. frequency at normal incidence for periods N = 1 to 6. The sample dimensions are specified in the caption of Fig. 5, open area 19%, aluminum plates ($l_a = 1.2$ mm thick) separated by air gaps ($l_b = 12.8$ mm thick).

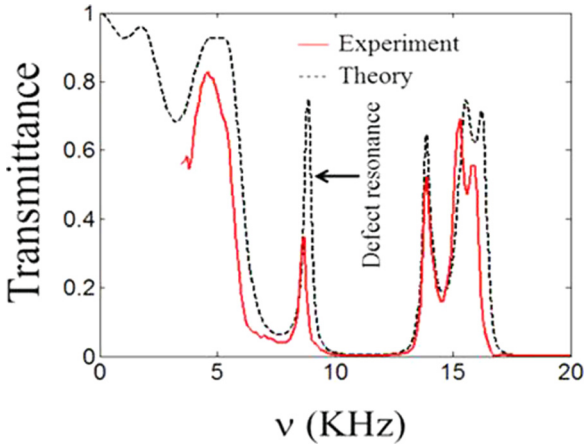

FIG. 7. Transmittance vs. frequency for the N = 4 period structure with an air defect layer in the center.

An important observation from Fig. 6 is that the transmittance of the multilayer stack significantly enhances the transmittance of a single plate. For example, at 15 kHz the transmittance is only 30% while the transmittance with a total of 5 plates is as high as 60%. Clearly, a resonant tunneling phenomenon is taken place due to the formation of an acoustic pass band in a spectral region of low transmission for the single layer.

For a single plate of acoustically hard material perforated with a periodic array of subwavelength 1-D slits or 2-D orifices, it is well-known that more sound passes through these subwavelength apertures than one would expect from simple geometrical considerations based on the aperture to period ratio. For example, in the current case the ratio of aperture size to the incident wavelength $\lambda/d = 17$ at 5 kHz. The phenomenon is known as extraordinary acoustic transmission (EAT) and it has been the subject of intense investigation in the past few years.[5,10–13] However, EAT is either achieved under some form of resonant condition[10–13] and is therefore limited in bandwidth and lossy, particularly in the case of very subwavelength apertures, or, as in the case of Ref. 5, can be achieved under broadband impedance matching condition at the intromission angle. Here, instead, we have experimentally demonstrated that EAT can be tailored basically at will with no bandwidth or angular limitations using the kinds of structures just described. Finally, in order to show the potentialities of such kinds of structures for sound manipulation, we have also tested an acoustic structure with an air defect layer of thickness $2l_b$ in the center, i.e., $MM(l_a)/air(l_b)/MM(l_a)/air(2l_b)/MM(l_a)/air(l_b)/MM(l_a)$, and found, as expected, a defect resonance close to the center of the first band gap, as shown in Fig. 7.

Many applications could be envisioned for such structures. For example, in analogy with the photonic case,[1,14] the presence of a band structure could make it possible to embed sound sources in the medium and quench their emission rates at the frequencies falling in the band gaps, while enhancing their emission rates at the band edges or near the defect resonances. "Slow"/"fast" sound propagation[15,16] at the band-edge/band-gap can be achieved analogously to the "slow"/"fast" light propagating in a photonic structure.[17] In particular, this approach can also be used for acoustic emission control by enhancing and suppressing emission of an acoustic source through the modification of the acoustic mode density. An acoustic emitter placed inside the structure cannot radiate at frequencies inside the gap thereby creating an "acoustic vacuum" at those frequencies. Preliminary experimental investigations we are currently conducting seem to confirm those claims and will be the subject of future communications.

Other applications may include sub-wavelength acoustic imaging, acoustic field concentration, harvesting, and impedance matching for multiple applications including medical diagnostics[18] and noise control.[19] This idea can also be extended to make an acoustic absorber by replacing one of layers (air) with an acoustically absorptive layer. While we have focused primarily on audible frequencies, this concept can also be extended to phonons for thermal management that is particularly important for thermoelectric materials where low thermal conductivity while maintaining high electrical conductivity[20] is desirable.

[1]J. D. Joannopoulos, R. D. Meade, and J. N. Winn, *Photonic Crystals, Molding the Flow of Light* (Princeton University Press, 1995).
[2]M.-H. Lu, L. Feng, and Y.-F. Chen, Mater. Today **12**, 34 (2009), and references therein.
[3]M. S. Kushwaha, Appl. Phys. Lett. **70**, 3218 (1997).
[4]M. Shen and W. Cao, J. Phys. D: Appl. Phys. **33**, 1150 (2000).
[5]G. D'Aguanno, K. Q. Le, R. Trimm, A. Alù, N. Mattiucci, A. D. Mathias, N. Akozbek, and M. J. Bloemer, Sci. Rep. **2**, 340 (2012).
[6]A. Maurel, S. Felix, and J. F. Mercier, Phys. Rev. B **88**, 115416 (2013).
[7]D.-X. Qi, R.-H. Fan, R.-W. Peng, X.-R. Huang, M.-H. Lu, X. Ni, Q. Hu, and M. Wang, Appl. Phys. Lett. **101**, 061912 (2012).
[8]P. Yeh, *Optical Waves in Layered Media* (Wiley, New York, 1988).
[9]D. T. Blackstock, *Fundamentals of Physical Acoustics* (John Wiley & Sons, Inc., New York, 2000).
[10]M.-H. Lu, X.-K. Liu, L. Feng, J. Li, C.-P. Huang, Y.-F. Chen, Y.-Y. Zhu, S.-N. Zhu, and N.-B. Ming, Phys. Rev. Lett. **99**, 174301 (2007).
[11]X. Wang, J. Appl. Phys. **108**, 064903 (2010).
[12]J. Christensen, L. Martin-Moreno, and F. J. Garcia-Vidal, Phys. Rev. Lett. **101**, 014301 (2008).
[13]H. Estrada, F. J. Garcıa de Abajo, P. Candelas, A. Uris, F. Belmar, and F. Meseguer, Phys. Rev. Lett. **102**, 144301 (2009).
[14]M. D. Tocci, M. Scalora, M. J. Bloemer, J. P. Dowling, and C. M. Bowden, Phys. Rev. A **53**, 2799 (1996).
[15]W. M. Robertson, C. Baker, and C. Brad Bennett, Am. J. Phys. **72**, 255 (2004).
[16]W. M. Robertson, J. Pappafotis, P. Flannigan, J. Cathey, B. Cathey, and C. Klaus, Appl. Phys. Lett. **90**, 014102 (2007).
[17]G. D'Aguanno, N. Mattiucci, M. Scalora, M. J. Bloemer, and A. M. Zheltikov, Phys. Rev. E **70**, 016612 (2004).
[18]S. Rhee, T. A. Fitter, K. K. Shung, H. Wang, and W. Cao, in *Proceedings of the IEEE Ultrasonics Symposium* (2001), p. 1051.
[19]J. P. Arenas and M. J. Crocker, "Recent Trends in Porous Sound-Absorbing Materials," Sound & Vibration (July 2010), available at http://www.SandV.com.
[20]L. Yang, N. Yang, and B. Li, Sci. Rep. **3**, 1143 (2013).